Organic Geochemistry 151 (2021) 104164

Contents lists available at ScienceDirect

Organic Geochemistry

journal homepage: www.elsevier.com/locate/orggeochem

Composition and lability of photochemically released dissolved organic matter from resuspended estuarine sediments

Jennifer L. Harfmann [a,*], G. Brooks Avery Jr. [a], Hugh D. Rainey [a], Ralph N. Mead [a], Stephen A. Skrabal [a], Robert J. Kieber [a], J. David Felix [b], John R. Helms [c], David C. Podgorski [d]

[a] Department of Chemistry and Biochemistry, University of North Carolina Wilmington, Wilmington, NC 28403, United States
[b] Department of Physical and Environmental Sciences, Texas A&M University – Corpus Christi, Corpus Christi, TX 78412, United States
[c] Department of Natural and Mathematical Sciences, Morningside College, Sioux City, IA 51106, United States
[d] Department of Chemistry, University of New Orleans, New Orleans, LA 70148, United States

ARTICLE INFO

Article history:
Received 22 June 2020
Received in revised form 13 November 2020
Accepted 18 November 2020
Available online 23 November 2020

Keywords:
Dissolved organic matter
Photo-release
Lability
Sediment
Resuspension
Estuarine

ABSTRACT

Photochemically-released dissolved organic matter (PR-DOM) from resuspended sediments is an understudied flux of dissolved organic carbon (DOC) and nutrients with the potential to influence estuarine microbial food webs. There is currently limited knowledge on the composition, lability and biological alterations of this material once released into the water column. This study addresses the composition and fate of PR-DOM from resuspended sediments of the Cape Fear River Estuary (CFRE) in southeastern North Carolina. Six-hour irradiation released 22–44% more DOC, and PR-DOM was of a different composition and enhanced lability, relative to dark controls. Irradiation led to release of humic-like DOM, indicated by increased chromophoric and fluorescent dissolved organic matter, substantial increases in the humification index, and production of oxidized higher molecular weight compounds with higher aromaticity, relative to dark controls. However, DOM of lower molecular weight and reduced aromaticity was produced as well. This was indicated by increased spectral slope ($S_{275-295}$) and decreased specific ultraviolet absorbance at 254 nm ($SUVA_{254}$), relative to dark controls. This latter pool of DOM may be linked to nitrogen-(N-) and sulfur-(S-)containing compounds that were photodegraded or biologically altered during irradiation experiments. In subsequent lability incubation experiments, degradation of PR-DOM was more rapid than DOM released from dark controls, especially for marine humic-like fluorophores. Incubation of PR-DOM led to an 8-fold increase in compounds with molecular formulas that were unique to light-exposed DOM relative to unexposed DOM, the majority of which were N- and S-containing compounds. Given that coastal sediments are typically enriched in these nutrients, N- and S-containing compounds appear to influence the lability of PR-DOM from estuarine resuspended sediments. Estimated lability of photoreleased DOC from resuspension events in the CFRE is comparable to previous bioavailable DOC estimates and suggests that episodic photochemical interactions with sediments may act as a previously unrecognized source of labile DOC to bacteria and plankton in these coastal waters.

1. Introduction

Understanding the chemical transformations, sources and sinks of dissolved organic matter (DOM) in coastal waters is vital in connecting biogeochemical cycles with trophic food webs in estuarine ecosystems. Resuspended estuarine sediments exposed to sunlight photolysis have been identified as a potential source of dissolved organic carbon (DOC) and nutrients to marine food webs (Kieber et al., 2006a; Mayer et al., 2006; Shank et al., 2011; Southwell et al., 2011). Estuarine environments are subject to both natural and anthropogenic resuspension of sediments into the water column, induced by highly energetic events such as hurricanes, thunderstorms, tidal movements, shipping activities and high winds. Additionally, modest wind conditions can resuspend sediments at a lesser intensity, but at a higher frequency (Blanton et al., 1999; Booth et al., 2000). Inorganic nutrients produced through resuspension-induced photochemical release are likely utilized quickly in the photic zone of coastal waters via the microbial loop (Azam et al., 1983; Southwell et al., 2011). However, less is known about the composition and biogeochemical fate of photoreleased

* Corresponding author.
E-mail address: harfmannj@uncw.edu (J.L. Harfmann).

https://doi.org/10.1016/j.orggeochem.2020.104164
0146-6380/

dissolved organic matter (PR-DOM), particularly as it relates to trophic food webs.

The majority of studies involving PR-DOM conclude that this material enhances microbial activity in the ocean (Mopper and Kieber, 2002; Mopper et al., 2015; Cory and Kling, 2018). In suspended sediments, knowledge of the extent of bioavailability of PR-DOM is inconclusive and the corresponding studies lack detailed chemical analyses of DOM transformations to parse out these inconsistencies (Mayer et al., 2011; Schiebel et al., 2015).

Natural DOM is an exceedingly complex mixture of organic compounds and the analytical tools to capture this complexity continue to evolve. Traditional spectroscopic analyses reveal photochemical production of chromophoric dissolved organic matter (CDOM) and fluorescent dissolved organic matter (FDOM) and imply the photochemical dissolution of DOM from coastal sediments (Shank et al., 2011; Schiebel et al., 2015). High molecular weight DOM that is ubiquitous in natural waters and chromophoric in nature, have received considerable attention (Coble, 1996; Kowalczuk et al., 2003; Stedmon and Nelson, 2015; Cheng et al., 2019); still, much of the molecular composition of this DOM has not been well characterized. Pairing optical techniques with higher resolution methods, such as Fourier transform ion cyclotron resonance mass spectrometry (FT-ICRMS), provides two potentially distinct analytical windows for characterizing this DOM and for visualizing abiotic and biotic transformation processes (Brogi et al., 2018). Studies combining spectroscopic analyses with FT-ICRMS indicate that photochemical degradation of estuarine DOM is a major removal mechanism for high molecular weight, terrestrially derived DOM, as water moves through an estuarine system (Stubbins et al., 2010; Seidel et al., 2015). However, DOM released from irradiation of resuspended sediments is potentially of an entirely different composition to bulk estuarine DOM and may impact estuarine food webs in unpredictable ways.

The goals of the current study were to: 1) characterize the optical and molecular composition of PR-DOM from resuspended estuarine sediments, and 2) examine the lability of PR-DOM relative to dark controls. This study offers new insight into the cycling of DOM, revealing a potentially under-studied and poorly quantified source of labile DOC that could contribute labile substrates to lower oceanic trophic levels.

2. Materials and methods

2.1. Study site and sampling

Sediment samples were collected in September 2014 in the Cape Fear River Estuary (CFRE), North Carolina, Wilmington, NC, USA (Fig. 1). Sites CFRE-1 (34.0335 °N, 77.937 °W; ~10 miles from sea) and CFRE-2 (34.1938 °N, 77.9573 °W; ~21 miles from sea) were chosen to coincide with sites studied by the Lower Cape Fear River Program, a well-established water quality monitoring program (Mallin et al., 2015). Sediment samples were collected from the top 2–3 cm using a Ponar grab sampler and placed in Ziploc bags and transported back to the laboratory in a cooler. Samples were stored at 4 °C for no longer than 1 month prior to initiating experiments. Seawater used in resuspensions was collected as a surface grab sample in the Gulf Stream (GSSW; 33.8722° N, 77.091 °W) on September 22nd, 2014 in 4 L high density polyethylene bottles and filtered with 0.2 μm polyethersulfone filters. Gulf Stream seawater was chosen as the resuspension matrix in order to provide a low DOC background and to mimic near offshore conditions in the case of a large resuspension event (Southwell et al., 2011).

2.2. Resuspension of sediments and irradiation

Sediment from CFRE-1 (0.8% OC) and CFRE-2 (0.7% OC) was size-fractionated in Gulf Stream seawater to obtain the fine sediment (<10–20 μm nominal diameter). This size range is environmentally relevant, given the penetration depth of photosynthetically active radiation (PAR) in the Cape Fear River Estuary of 1.3–2.4 m (R.F Whitehead, pers. comm.). Kieber et al. (2006b) demonstrated that while UV wavelengths were most effective at initiating DOC photorelease from particles, PAR, which penetrates to these deeper depths, also plays a role. Given a settling velocity of estuarine suspended particles of 0.0001 m s^{-1} (Hill et al., 2000), particles of <10–20 μm diameter could remain suspended for roughly 4–7 h within the upper 2.4 m of the Cape Fear water column. Preliminary size-fractionation experiments were performed to identify appropriate sediment mass/volume ratios that would target total suspended solids (TSS) concentrations of 160 mg L^{-1}, within the range found in many estuarine environments (Zhang, 1999; Perez et al., 2000; Yang et al., 2020). To size-fractionate sediments, ~5–6 g (wet weight) of each sample was placed into 4 L of filtered seawater. The resulting mixture was vigorously agitated for 1–2 min and allowed to settle for 40 min in order to exclude coarse particulate matter. The top 20 cm of the mixture (corresponding to sediment <ca. 10–20 μm according to Stokes' Law) (Jackson, 1973) was then siphoned by pipette from the center of the 4 L container into two separate 1 L quartz round bottom flasks and placed in a solar simulator for irradiation. An analogous flask was wrapped in aluminum foil and placed next to the light sample inside the solar simulator to act as a dark control. Samples were placed on a Gyrotory® shaker model G2 set at 100 RPM to keep sediments suspended throughout the experiment, and flasks were periodically rotated to ensure homogenous light exposure. An additional sample was placed in a combusted flask and immediately filtered (Whatman GF/F filter) for DOC and optical analysis as an initial sample.

Samples were irradiated for six hours using a solar simulator (Spectral Energy solar simulator LH lamp housing with a 1000 W Xe arc lamp) equipped with a sun lens diffuser and an AM1 filter to remove wavelengths not found in the solar spectrum. Irradiance conditions followed those of previous resuspended sediment photolysis experiments (Kieber et al., 2006b, 2017; Southwell et al., 2011; Helms et al., 2014; Avery et al., 2017; Skrabal et al., 2018). While laboratory irradiance allowed for a more consistent and measurable light field than natural sunlight, the tradeoff was limited space in the solar simulator, which prevented the replication that field experiments could offer. All quartz and glassware used were rinsed with high-purity water (≥18.2 MΩ cm; Milli-Q Reference system, Millipore Corp) and combusted at 450 °C for at least 4 h prior to use. Samples were filtered following irradiation through a combusted 47 mm Whatman GF/F filter and a subset was prepared for DOC and optical analysis.

Molecular level changes in PR-DOM were assessed using FT-ICRMS in separate irradiation experiments using CFRE-2 sediment (Supplemental Figure A). While optical analyses were performed on both CFRE-1 and CFRE-2, FT-ICRMS was limited to one site due to finite resources and the similarity in organic carbon content of CFRE-1 and CFRE-2. These separate irradiation experiments were identical to the above except approximately 1.7 g (wet weight) was added to 2 L filtered seawater in a Teflon bottle and allowed to settle for 17.5 min. The upper 10 cm of the mixture was then siphoned into quartz tubes for 6 hour irradiation. Despite potential differences in TSS between the two sets of experiments, both methods targeted sediments < ca. 10–20 μm.

2.3. DOC lability incubation experiments

Following the primary irradiation experiment, approximately 950 mL of each GF/F filtered sample was placed into a combusted 4 L glass container with a freshly collected seawater inoculum (4% v:v), capped, and incubated in the dark for approximately 30 days.

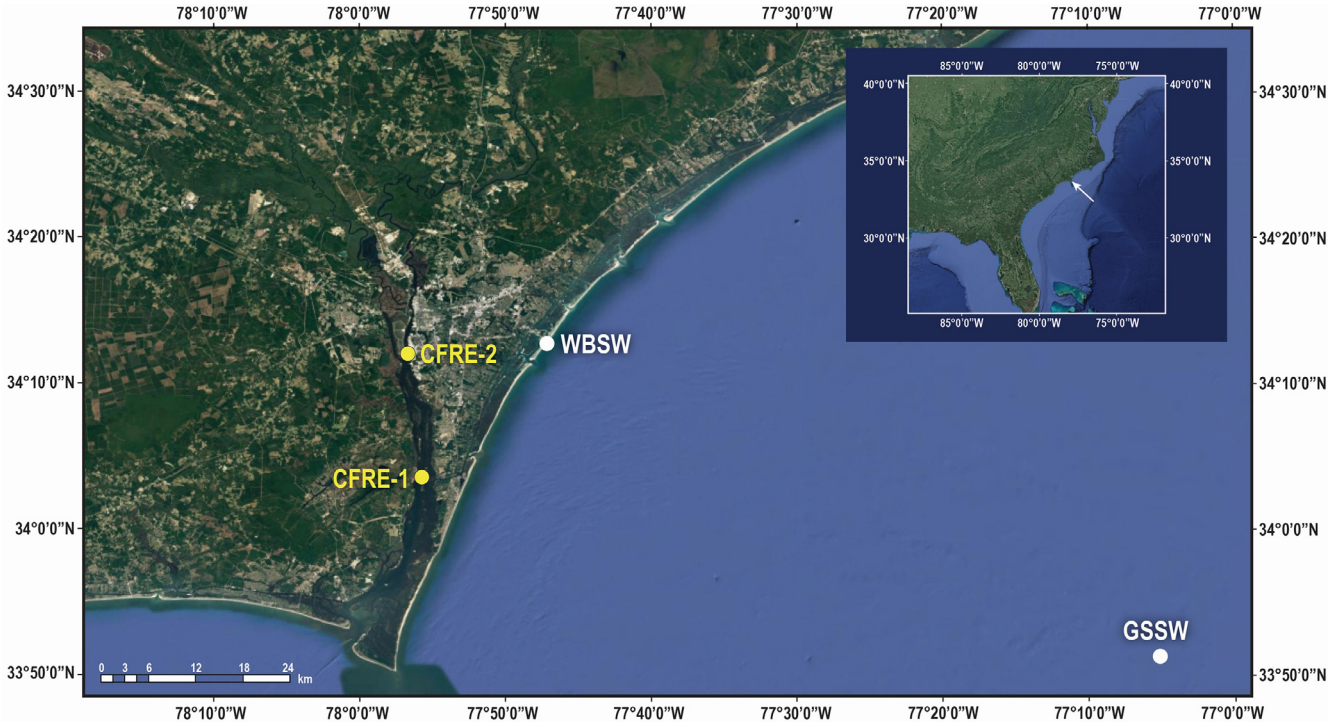

Fig. 1. Map of collection sites for sediments in the lower Cape Fear River, NC, USA (yellow; CFRE-1 and CFRE-2) and nearby seawater (white; GSSW and WBSW). (For interpretation of the references to color in this figure legend, the reader is referred to the web version of this article.)

Herein, lability incubation samples are referred to as either unexposed (sediments from 'dark' irradiation treatment) or light-exposed (sediments from 'light' irradiation treatment) to distinguish samples derived from the lability incubation from those derived from the irradiation experiments.

Seawater for inoculum was collected just offshore of Wrightsville Beach, North Carolina (WBSW; 34.2085° N, 77.7964 °W) to simulate bacterial and plankton communities near sediment sites. Seawater was screened through a 100 μm net to remove larger grazing organisms and particles while keeping most of the bacterial community intact (Herlemann et al., 2014). Samples for the CFRE-2 site were taken on days 0, 2, 5, 11, 22, and 30 after irradiation and filtered (47 mm Whatman GF/F) for DOC and optical analyses. Samples for CFRE-1 were sampled less frequently – on days 0, 10, 20, and 29 – allowing for sufficient final sample volume to assess molecular level changes via FT-ICRMS in addition to DOC and optical analyses.

DOC and optical parameter measurements were normalized to values at the start of each incubation and are presented as percent loss. Photo-enhanced lability was assessed as differences between normalized parameters in unirradiated and light-exposed treatments. The term 'lability' is used rather than 'bioavailability', in the current study to acknowledge that abiotic mechanisms such as hydrolysis may contribute to a small degree to observed differences.

2.4. DOC analysis

Dissolved organic carbon was determined by high temperature combustion (HTC) using a Shimadzu TOC total organic carbon analyzer equipped with an ASI-L autosampler (Shimadzu, Kyoto, Japan). Standards were prepared from reagent grade potassium hydrogen phthalate (KHP) in high-purity water (≥18.2 MΩ cm; Milli-Q Reference system, Millipore Corp). Samples and standards were acidified to pH 2 with 6 M HCl and purged to remove inorganic carbon. DOC concentrations are reported as an average of triplicate injections.

2.5. Absorption analysis

Absorption measurements were made on a double beam spectrophotometer (Cary 100 Bio UV–Visible Spectrophotometer) with a 1 cm quartz cell, and high-purity water (≥18.2 MΩ cm; Milli-Q Reference system, Millipore Corp) was used as the blank. All scans were made from 200 to 800 nm at 1 nm intervals. Absorption coefficients of filtered samples, a_λ, were calculated using the equation $a_\lambda = 2.303\ A_\lambda/l$ where A_λ is the corrected spectrophotometer absorbance reading at wavelength λ and l is the optical pathlength in meters. All absorption measurements were corrected for instrument drift and scattering by subtracting the average absorbance in the spectral range from 725 to 775 nm (Helms et al., 2008). Samples were also corrected for inner filter effects when absorbance at 254 nm exceeded 0.05. The absorption coefficient at 300 nm (a_{300}) was used as an index for CDOM abundance (Del Castillo et al., 1999; Kieber et al., 2006a). The specific UV absorbance of the DOC calculated at 254 nm ($SUVA_{254}$) was determined by normalizing the decadic absorption coefficient at 254 nm with DOC concentration and is reported in units of liter per milligram carbon per meter ($L{\cdot}mg\ C^{-1}{\cdot}m^{-1}$) (Weishaar et al., 2003). Spectral slope ($S_{275-295}$) was calculated using linear regression of the log-transformed UV absorbance spectra between 275 and 295 nm with $R^2 > 0.98$ (Helms et al., 2008). In contrast to DOC, absorbance measurements are reported without boundaries of analytical precision since instrument variability is negligible for the double-beam spectrophotometer.

2.6. Fluorescence analysis

Three dimensional excitation-emission matrix (EEM) fluorescence measurements were made using a Horiba Aqualog 3D fluo-

rometer equipped with a 150 W ozone-free Xe arc lamp and a multichannel charge coupled device (CCD) detector. Excitation wavelengths ranged from 240 to 600 nm at 3 nm increments, whereas emission wavelengths were collected in a range from 212 to 621 nm at 3 nm increments. All EEM intensities were blank-subtracted using high-purity water, Raman and Rayleigh scatter corrected, and corrected for the inner-filter effect using Origin 8.1 Aqualog software. All corrections were performed prior to normalization to quinine-sulfate-unit equivalents (QSE). The instrument was calibrated based on the excitation at 347.5 nm of 1 ppb quinine sulfate dihydrate dissolved in 0.1 M perchloric acid, with measurement of the intensity at 450 nm. Scans were corrected by a UV-enhanced silicon photodiode reference detector to account for changes in lamp output.

In addition to total FDOM integrated over each EEM, fluorescent regions in the EEMs spectra were identified using the letter system (A, C, M, T) first proposed by Coble (1996). The A peak is humic-like and absorbs strongly in the UV region, indicating it is less aromatic in nature. The C peak is also humic-like but absorbs more strongly in the visible region and is comparatively more aromatic. The M peak is associated with marine humic-like substances and may be a possible photoproduct of carbon (Kieber et al., 2006a). The T region is indicative of protein-like fluorophores, such as tryptophan and tyrosine. These component peaks were integrated by rectangle in Excel based on the free-form integration parameters set forth by Kieber et al. (2006a). Fluorescence index (FI) was determined as the ratio of emission wavelengths at 470 and 520 nm obtained at excitation wavelength 370 nm (McKnight et al., 2001). Humification index (HIX) was calculated as the area under the emission spectra 435–480 nm divided by the peak area 300–345 nm + 435–480 nm at excitation wavelength 254 nm (Ohno, 2002). Biological index (BIX) was calculated as the ratio of emission intensity at 380 nm divided by 430 nm at excitation wavelength 310 nm (Huguet et al., 2009). As with absorbance, fluorescence measurements are reported without boundaries of analytical precision given stability in fluorometer readings.

2.7. FT-ICRMS analysis

Samples were prepared for FT-ICRMS analyses with Agilent Bond Elut PPL solid-phase extraction (SPE) cartridges filled with 500 mg of functionalized styrene–divinylbenzene polymer (PPL) resin (Dittmar et al., 2008). The SPE cartridge was conditioned with 3 mL of methanol and 3 mL of methanol:acetonitrile (1:1). Approximately 170 mL of sample was passed through the cartridge. The cartridge was then washed with one cartridge volume (3 mL) of methanol:high-purity water (1:100). It was then dried under N_2 gas and sample was eluted with three 1 mL fractions of methanol:acetonitrile (1:1). Samples were ionized by electrospray ionization in the negative mode, (−) ESI, and analyzed with a 9.4 T FT-ICR mass spectrometer located at the National High Magnetic Field Laboratory (NHMFL; Tallahassee, FL) (Blakney et al., 2011; Kaiser et al., 2011). A "walking" calibration method with homologous series of high abundance was utilized for internal calibration of each spectrum (Savory et al., 2011). EnviroOrg™ software developed at the NHMFL was used for molecular formula assignment and data visualization. Reproducibility for individual samples on multiple different ultrahigh resolution MS platforms is reported in detail by Hawkes et al. (2020).

Molecular formulas unique to each treatment were extracted and grouped by element class (CHO, CHON, CHOS) and compound class (condensed aromatics, polyphenols, unsaturated low oxygen, unsaturated high oxygen, aliphatics, and peptide-like). Compound classes were defined by elemental ratio and modified aromaticity index (Koch and Dittmar, 2006) as outlined in Spencer et al. (2014). Unique molecular formula distributions were also assessed across several common FT-ICRMS metrics, including oxygen class (O class), nitrogen class (N class), nominal oxidation state of carbon (NOSC) as in Riedel et al. (2012), modified aromaticity index (AI_{mod}) as in Koch and Dittmar (2006), and double bond equivalents minus oxygen (DBE-O) as in Gonsior et al. (2009). AI_{mod} corrects for the decreased pi bonding observed in marine DOM (Koch and Dittmar, 2006), and DBE-O excludes carboxyl group contributions to DBE, thereby more accurately representing unsaturation of the carbon skeleton (Gonsior et al., 2009).

3. Results

3.1. Photo-induced alteration of DOM from resuspended sediments

3.1.1. DOC and optical effects

Initial DOC concentrations were 101 ± 1 μM and 80 ± 1 μM for CFRE-1 and CFRE-2, respectively. DOC remained relatively unchanged in dark controls, but increased to 123 ± 2 μM and 115 ± 3 μM in light treatments. Correspondingly, 22 ± 2% and 44 ± 4% more DOC was released in light treatments relative to initial DOC for CFRE-1 and CFRE-2, compared to only 5 ± 1% and 1 ± 2% more DOC released in dark controls (Table 1). Irradiation therefore resulted in up to 43% more DOC release than dark controls. CFRE-2 exhibited higher net photo-release than CFRE-1, but release of CDOM and FDOM were enhanced upon light exposure for both sites, with a_{300} and total FDOM increasing nearly tenfold compared to dark control samples (Table 1). Net photo-release of FDOM was attributed primarily to peak A, with additional contribution from peaks C and M (Table 2). Changes in optical indices were also enhanced in irradiated samples. $SUVA_{254}$ decreased 61–76% upon irradiation, and $S_{275-295}$ increased 6–14% (Table 1). While the change in FI due to irradiation was minimal, HIX increased by 90–210% after irradiation and BIX decreased by 26% (Table 1).

3.1.2. Molecular level changes

Molecular differences between dark and light treated samples were highlighted by considering only the molecular formulas unique to each sample set. Compared to dark controls, light treatments produced more compounds with molecular formulas with a higher average molecular weight (dark: 1066 compounds, mean = 423 Da; light: 1347 compounds, mean = 481 Da) (Fig. 2).

Table 1
Percent change (Δ%)[1] in DOC and optical parameters following 6 hour irradiation of resuspended sediments.

Parameter	Site	Dark	Light
DOC	CFRE-1	5 ± 1	22 ± 2
	CFRE-2	1 ± 2	44 ± 4
a_{300}	CFRE-1	−8	177
	CFRE-2	25	250
$SUVA_{254}$	CFRE-1	5	−61
	CFRE-2	−40	−76
$S_{275-295}$	CFRE-1	3	6
	CFRE-2	4	14
Total FDOM	CFRE-1	7	90
	CFRE-2	31	186
FI	CFRE-1	−2	−17
	CFRE-2	−17	−15
HIX	CFRE-1	−2	90
	CFRE-2	56	210
BIX	CFRE-1	3	−26
	CFRE-2	−7	−26

[1] $\Delta\% = \left(\frac{X_f - X_i}{X_i}\right)(100)$ where X_i = value prior to irradiation and X_f = value following irradiation.

Table 2
Net photo-release of DOC and changes to optical parameters following 6 hour irradiation of resuspended sediments. Positive values indicate an increase in the light treatment.

Parameter	Site	Net Photo-Release[1]
DOC (μM)	CFRE-1	27 ± 2
	CFRE-2	34 ± 3
a_{300} (m^{-1})	CFRE-1	2.4
	CFRE-2	2.7
Total FDOM (QSE)	CFRE-1	58.3
	CFRE-2	78.6
Peak A (QSE)	CFRE-1	16.5
	CFRE-2	21
Peak C (QSE)	CFRE-1	5.6
	CFRE-2	8.8
Peak M (QSE)	CFRE-1	7.3
	CFRE-2	9.8
Peak T (QSE)	CFRE-1	−0.5
	CFRE-2	1.3

[1] Net photo-release = $X_L - X_D$ where X_L = value after 6-hr photo-exposure and X_D = value in corresponding dark control.

CHO compounds comprised 43–52% of all unique molecular formulas, and while the number of unique CHO compounds was similar for both treatments, those in the light treatment had higher O:C and lower H:C ratios, compared to those of the dark control (Fig. 3). Similarly, for CHON, dark and light treatments exhibited comparable proportions of unique formulas (31–35%, Fig. 2) but those in the light treatment had much higher O:C ratios (Fig. 3). CHOS compounds comprised the smallest percentage of unique molecular formulas, but were twice as prevalent in the light treatment compared to the dark control (Fig. 2) and followed trends of low H:C and high O:C relative to dark controls (Fig. 3). The percent of unique unsaturated high O compounds in the light treatment was more than three times that of the dark treatment, and irradiation produced fewer aliphatic and slightly more peptide-like compounds relative to dark controls (Fig. 2).

Across all elemental classes (CHO, CHON, and CHOS), light treatments exhibited higher O class and NOSC than dark counterparts (Fig. 4). N class was particularly affected by irradiation, with roughly half of unique compounds in dark controls containing 1 N (43%) and half containing 2 N (57%), but all unique compounds in light treatments containing 1 N. Interestingly, for DBE-O and AI_{mod}, CHON and CHOS compounds exhibited opposite trends relative to CHO, decreasing in light treatments across these metrics (Fig. 4).

3.2. Lability incubation effects of photo-released DOM from resuspended sediments

3.2.1. DOC and optical effects

Bulk photo-released DOC (PR-DOC) was consistently more labile than unexposed DOC (Fig. 5a). Overall, lability incubations reduced DOC concentrations in light-exposed samples 15% and 17% for sites CFRE-1 and CFRE-2, respectively, while DOC in unexposed treatments was reduced 8% and 12%. Photo-enhanced lability of bulk DOC was in part attributed to FDOM. There was a 7–12% loss of total FDOM in pre-irradiated treatments compared to a 4% loss in unexposed treatments (Fig. 5b). While fluorophore peak A (associated with humic-like, degradation-resistant compounds) accounted for the majority of total FDOM (ca. 25%, Supplemental Table A), peaks M and T (associated with humic-like marine and protein-like compounds, respectively) exhibited the strongest photo-enhanced lability toward the end of the incubation, particularly for CFRE-1 (Fig. 6). Following incubations, peak M fluorescence decreased 13% in light-exposed treatments but less than 5% in unexposed treatments, and peak T fluorescence decreased 10–34% in light-exposed treatments but 0–18% in unexposed treatments.

Lability of CDOM in resuspended sediments appeared to be unaffected by irradiation (Supplemental Figure B). While there was a 0–20% loss in a_{300} across microcosms, variance throughout the incubation – particularly in the dark control – suggests that *in situ* transformations, such as bacterial or planktonic production or viral cell lysis, were more significant in driving this parameter than enhanced lability through irradiation, as suggested by Mayer et al (2011).

3.2.2. Molecular level changes

Light-exposed samples produced 8 times more unique molecular formulas than unexposed samples, including 924 unique CHOS compounds and 552 unique CHON compounds (Fig. 7). These data

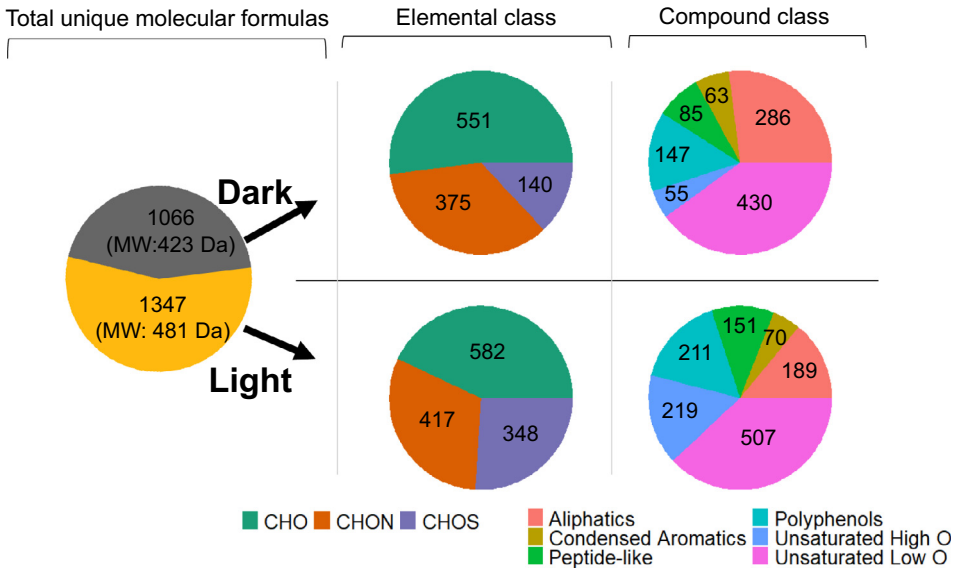

Fig. 2. Distribution of unique molecular formulas following irradiation of resuspended sediments (CFRE-2) as determined by (–) ESI FT-ICRMS. Number of unique molecular formulas is indicated for each class, as well as average molecular weight for all unique formulas.

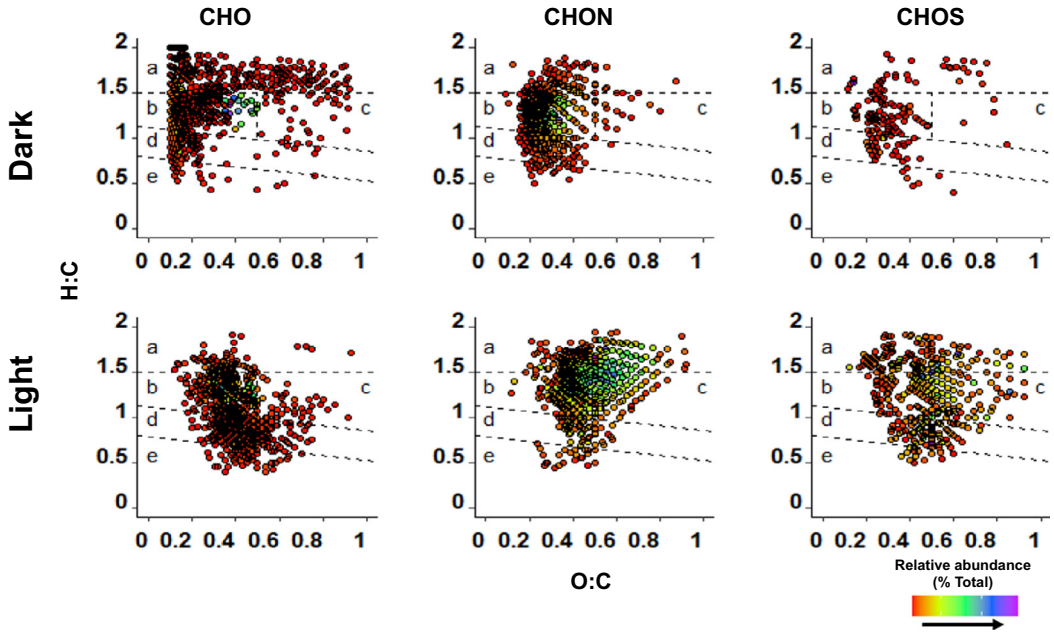

Fig. 3. Van Krevelen plot of molecular formulas determined by (−) ESI FT-ICRMS for dark control and light-exposed CFRE-2 resuspension mixture. Color indicates relative abundance, displayed as a percent of total unique formulas. Dotted lines are adapted from Kellerman et al. (2014) and represent estimated compound class delineations (a: aliphatic/peptide-like; b: unsaturated low oxygen; c: unsaturated high oxygen; d: polyphenols; e: condensed aromatics), though exact categorizations may differ slightly.

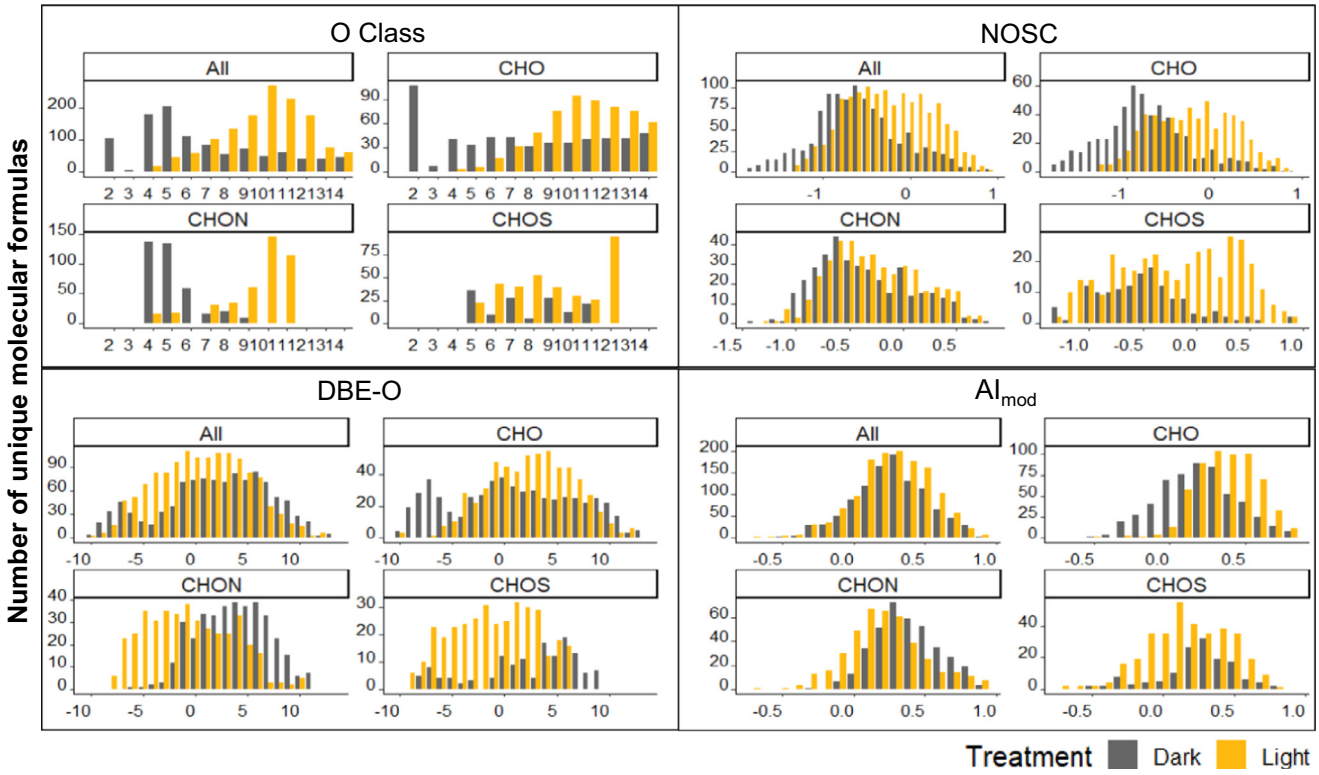

Fig. 4. Distribution of unique molecular formulas across several molecular parameters as determined by (−) ESI FT-ICRMS for dark (grey) and light (yellow) CFRE-2 resuspension mixture. O Class: oxygen class, NOSC: nominal oxidation state of carbon, DBE-O: double-bond equivalents minus oxygen, AI_{mod}: modified aromaticity index. (For interpretation of the references to color in this figure legend, the reader is referred to the web version of this article.)

represent production of compounds with unique molecular formulas and indicate significant diversification of the CHON and CHOS pools. H:C and O:C ratios of unique molecular formulas were comparable across both light-exposed and unexposed treatments (Fig. 8). Proportions of polyphenols, condensed aromatics, and unsaturated high oxygen compounds were higher in light-exposed samples, with relatively lower contributions of aliphatics and unsaturated low oxygen compounds (Fig. 7). In contrast to trends observed in irradiation experiments, unique molecular formulas in light-exposed incubation samples were, on average, of

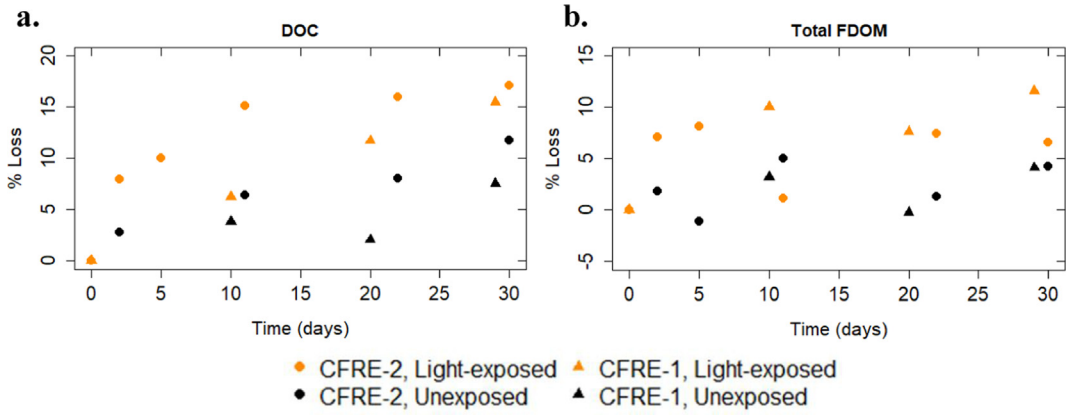

Fig. 5. Percent loss of a) dissolved organic carbon (DOC) and b) total fluorescence (total FDOM) of light-exposed (orange) and unexposed (black) microcosms of CFRE-1 (Δ) and CFRE-2 (O) sampling sites. (For interpretation of the references to color in this figure legend, the reader is referred to the web version of this article.)

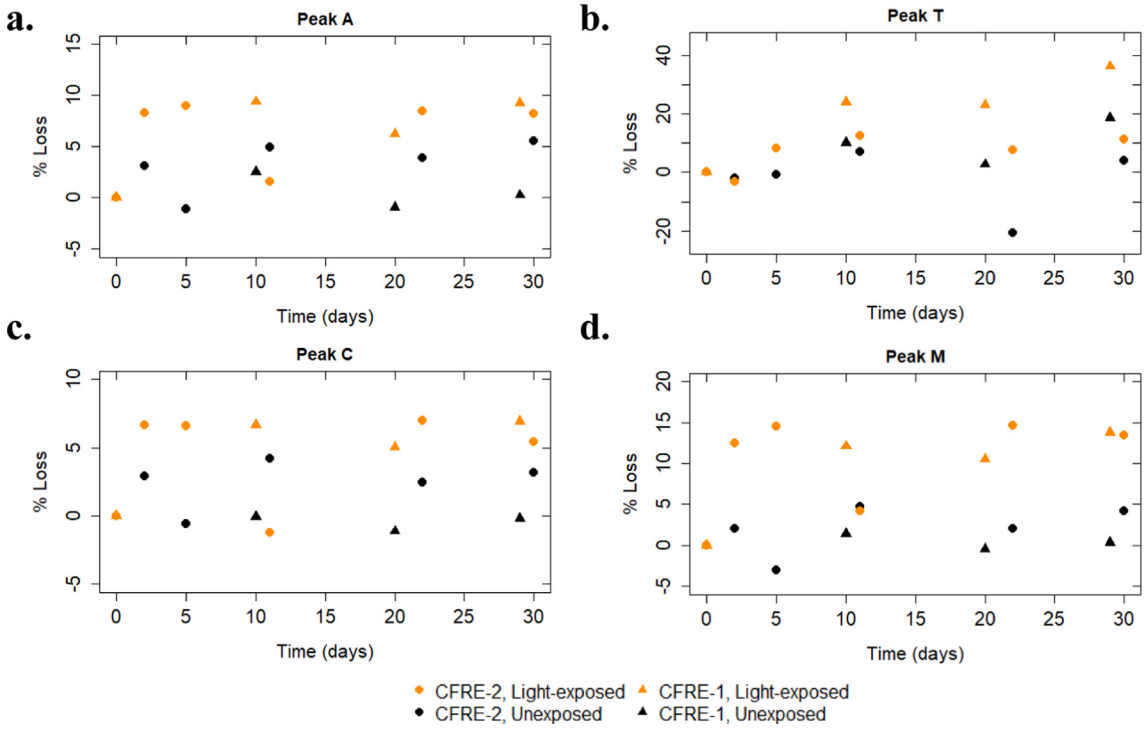

Fig. 6. Percent loss of a) Peak A, b) Peak T, c) Peak C, and d) Peak M of light-exposed (orange) and unexposed (black) microcosms of CFRE-1 (Δ) and CFRE-2 (O) sampling sites. (For interpretation of the references to color in this figure legend, the reader is referred to the web version of this article.)

lower molecular weight, decreased O class, increased DBE-O, increased AI_{mod}, and increased N class, relative to those of unexposed samples (Fig. 9). NOSC was the only metric that displayed similar trends in light treatments compared to dark controls across both irradiation experiments and incubations.

4. Discussion

4.1. Irradiation-induced transformations of DOM from resuspended sediments

As one of the primary drivers of DOM transformation in coastal systems, irradiation has the potential to alter DOM composition through either photohumification (bond making that leads to larger and/or more complex DOM), or photodegradation (bond breaking that leads to smaller and/or simpler DOM). Both photohumification and photodegradation have been observed in natural systems (Osburn et al., 2011; Lønborg et al., 2016) including resuspended sediments (Kieber et al., 2006b; Mayer et al., 2006; Shank et al., 2011; Southwell et al., 2011). Photorelease of sedimentary organic matter generally increases absorption properties in the dissolved phase through dissolution of aromatic and condensed moieties in the original particulate organic matter, as well as possible photohumification (Kieber et al., 1997). However, concurrent and subsequent photodegradation may either increase CDOM/FDOM through degradation of aromatic amino acids (Reche et al., 2001; Reitner et al., 2002), or decrease it through photooxidation and/or mineralization of aromatic compounds. The chemical composition of DOM dictates which transformation processes will dominate.

Release of humic or humic-like structures was a dominant transformation process during the irradiation of CFRE sediments,

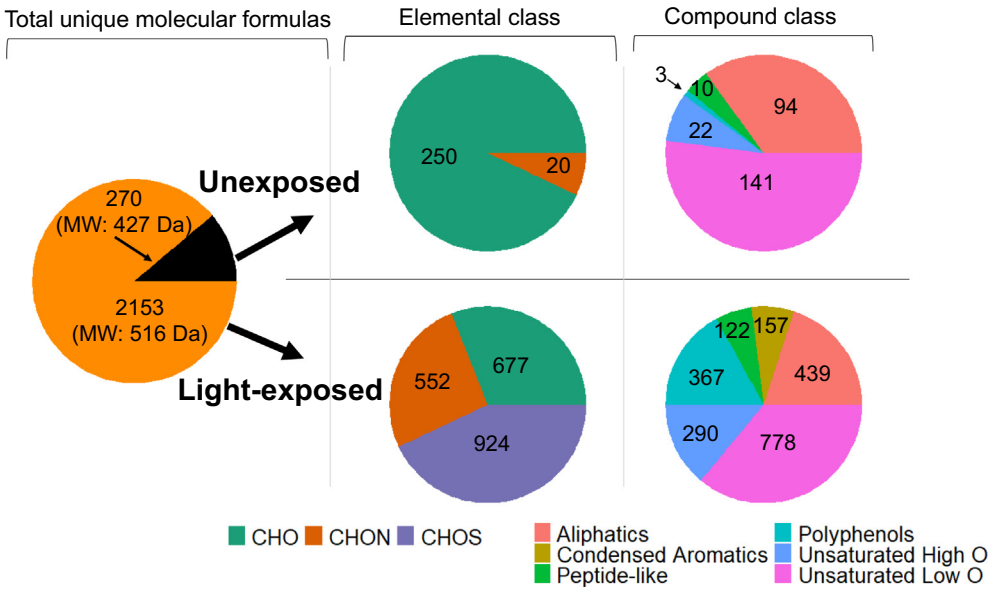

Fig. 7. Distribution of unique molecular formulas following lability incubation of resuspended sediments (CFRE-1) as determined by (−) ESI FT-ICRMS. Number of unique molecular formulas is indicated for each class, as well as average molecular weight for all unique formulas.

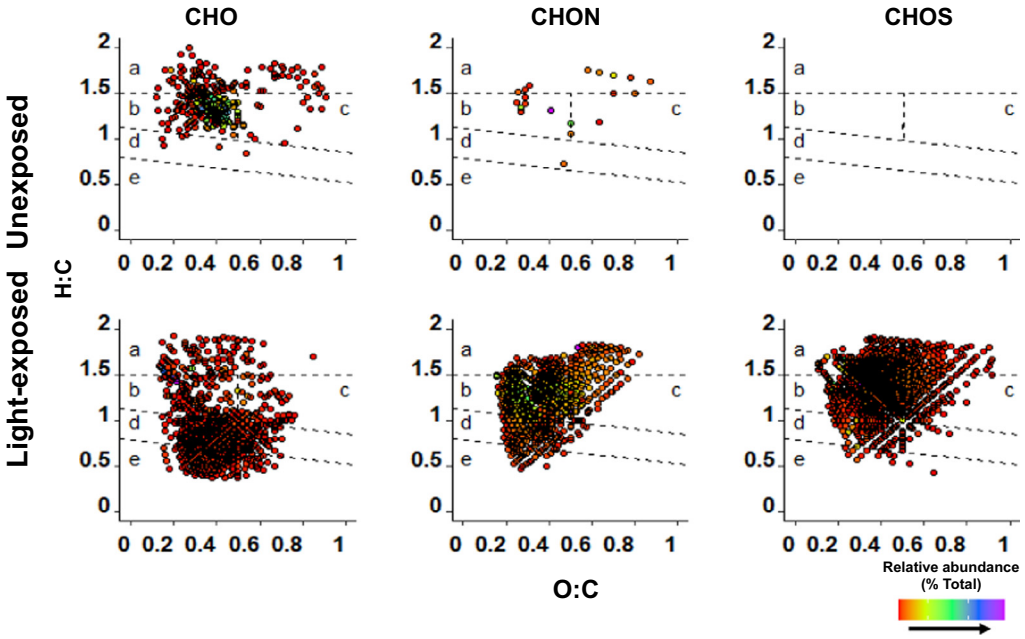

Fig. 8. Van Krevelen plot of molecular formulas determined by (−) ESI FT-ICRMS for unexposed and light-exposed CFRE-1 resuspension mixture following lability incubation. Color indicates relative abundance, displayed as a percent of total unique formulas. Dotted lines are adapted from Kellerman et al. (2014) and represent estimated compound class delineations (a: aliphatic/peptide-like; b: unsaturated low oxygen; c: unsaturated high oxygen; d: polyphenols; e: condensed aromatics), though exact categorizations may slightly differ.

as evidenced by substantial increases in HIX (Table 1). Optically active DOM was produced, and ionizable PR-DOM was of higher molecular weight and was more highly unsaturated than DOM released in dark conditions (Fig. 2). CHO compounds – which constituted roughly half of the DOM pool – had elevated DBE-O and AI_{mod}, indicating the production of aromatic compounds (Fig. 4). However, decreases in $SUVA_{254}$ and increases in $S_{275–295}$ suggest removal of aromatic compounds and shifts to lower molecular weight DOM (Table 1), reflecting alterations of non-CHO compounds. N- and S-containing PR-DOM had lower DBE-O and AI_{mod} and the molecular weight of S-containing compounds decreased with irradiation (Fig. 4). The N class was heavily impacted, with the complete elimination of higher N order compounds. Taken together, N- and S-containing compounds appeared to exhibit differing trends than photohumified CHO compounds. It is possible that N- and S-containing compounds may have been influenced by photodegradation instead of photohumification.

Alternatively, biological degradation may be driving changes in N- and S-containing compounds. Biodegradation could explain increases in peak A, C, and M FDOM, since metabolic byproducts are linked to FDOM in these regions (Biers et al., 2007). Biological processing likely contributed to irradiation-induced transformations in our study, as evidenced by the production of a significant number of unique molecular formulas in dark controls.

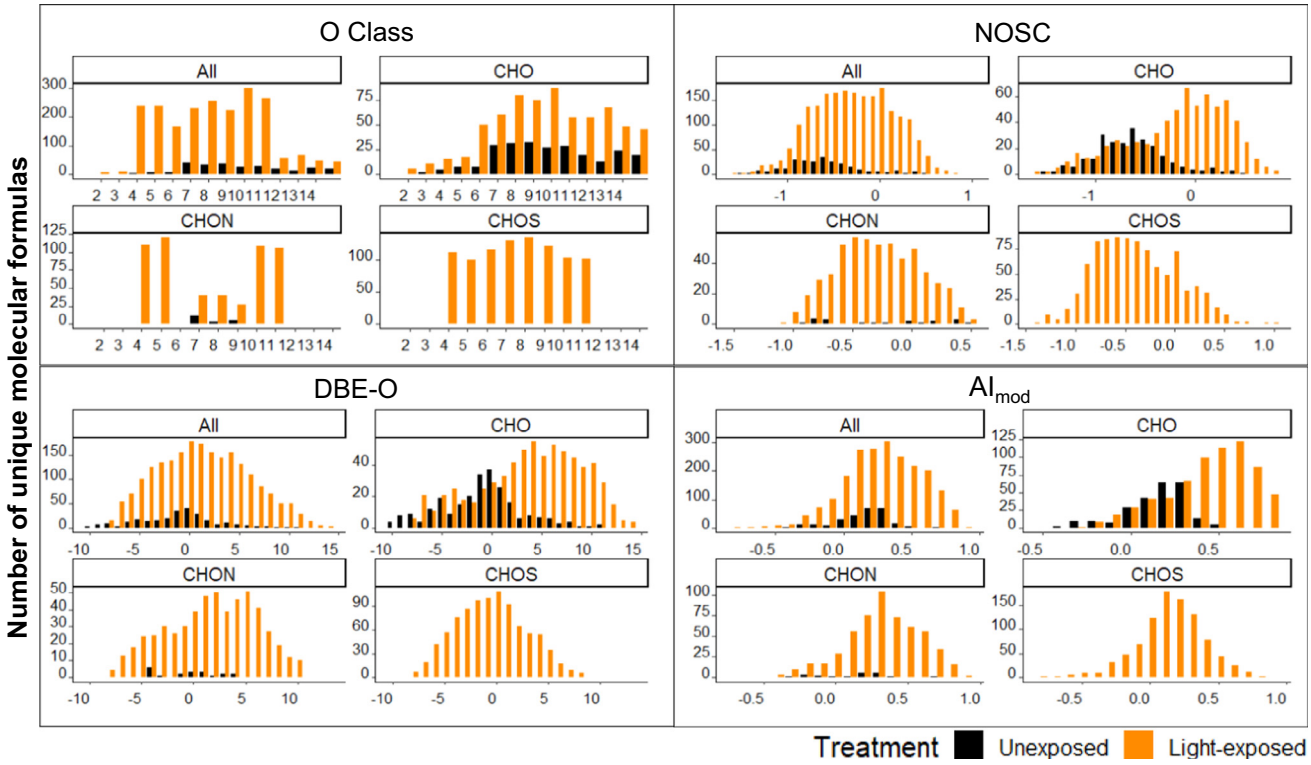

Fig. 9. Distribution of unique molecular formulas across several molecular parameters as determined by (–) ESI FT-ICRMS for unexposed (black) and light-exposed (orange) CFRE-1 resuspension mixture. O Class: oxygen class, NOSC: nominal oxidation state of carbon, DBE-O: double-bond equivalents minus oxygen, AI_{mod}: modified aromaticity index. (For interpretation of the references to color in this figure legend, the reader is referred to the web version of this article.)

Photochemical-biological coupling of DOM degradation is well-documented and can alter DOM more substantially than either process in isolation (Tranvik and Bertilsson, 2001; Judd et al., 2007; Cory et al., 2013). The transformations observed in the 6 hour irradiation presented here likely represent these synergistic effects that occur in DOM released from coastal sediment resuspension, and our data support the contention that bio-labile DOM was photoreleased from suspended CFRE sediments. Bacteria also release photo-labile DOM from particles (Hansell et al., 2009), but based upon the results presented here – at least for sunlit surface waters – the former process clearly outpaces the latter.

4.2. Lability of photo-released DOM (PR-DOM)

Irradiation-induced transformation processes, such as photodegradation and photohumification, may either enhance or suppress DOM lability to trophic food webs. In sediment resuspensions from Boston Harbor, up to 65% of PR-DOC and up to 100% of photoreleased dissolved organic N were bioavailable, but Florida sediments produced only 7% bioavailable PR-DOC, with no detection of bioavailable dissolved organic N (Schiebel et al., 2015). Mayer et al. (2011) reported that PR-DOM from Louisiana coastal sediments was up to 29% less bioavailable than algal detritus-derived DOM, although they also report 24 ± 38% more DOC loss in irradiated samples relative to controls. Discrepancies across studies are likely attributed to variability in sediment organic matter composition that translates into variability in PR-DOM composition, ultimately affecting irradiation-induced transformation processes.

In the current study, observed lability of PR-DOM (Fig. 6) may be attributed to differing composition of light-exposed samples relative to unexposed samples. The eight-fold increase in the number of compounds produced in light-exposed samples (Fig. 7) indicates substantial microbial influence on PR-DOM from CFRE sediments. In addition, NOSC was elevated in light-exposed DOM (Fig. 9) and is positively associated with thermodynamic favorability of microbial degradation (Boye et al., 2017). Oxygen content was a dynamic aspect of photo-alterations in this study, both in terms of oxygen class and O:C ratios. While oxygen content appears to be an important parameter for photo-alterations of DOM, its impact on biological lability is unclear. Elevated O:C ratios – such as those observed in light treatments (Fig. 3) – have been linked with both enhancement (Kim et al., 2006) and suppression of bacterial growth (Sun et al., 1997), and other studies found no evidence of correlation between bioavailability and oxygen content (Hunt et al., 2000).

N- and S-containing compounds, on the other hand, are highly relevant to lability. The number of unique CHON compounds increased from 7% in unexposed treatments to 26% in light-exposed treatments, and CHOS compounds increased from 0% to 43% (Fig. 7). Given low DBE-O and AI_{mod} relative to CHO compounds, lability of N- and S-containing PR-DOM is likely because these compounds were not as highly photohumified as CHO compounds, either due to photodegradation or biological transformation in irradiation experiments. Given that FT-ICRMS analyses for lability experiments were performed only on CFRE-1 - sediment that exhibited less photo-release than CFRE-2 sediments (Tables 1, 2) – environmental lability may be even higher, possibly linked to N and S content of the sediment. As previously mentioned, N-rich compounds are widely regarded as bioavailable, with amino acids constituting a large fraction of this bioavailable pool (Findlay and Sinsabaugh, 2003). N and S are abundant in coastal sediments (Seidel et al., 2015) with tidal inputs and sea spray a considerable source of S (Hertkorn et al., 2016), and many marine sedimentary bacteria utilize S-containing compounds for metabolism (Wasmund et al., 2017). N- and S-containing compounds may therefore play a disproportionately large role in the lability of photoreleased DOM from resuspended sediments in estuaries.

As with N- and S-containing compounds, FDOM in the T and M region were labile pools of DOM in this study, with increased loss of fluorescence intensity in both regions for light-exposed treatments relative to unexposed treatments (Fig. 6). The T region consists of protein-like fluorophores that are traditionally regarded as labile, although it may also include aromatic compounds such as lignin (Hernes et al., 2009). The T peak was the only fluorophore to decrease with photo-exposure in irradiation experiments (Table 2), indicating high photoreactivity that would limit its relevance for lability in the natural environment. On the other hand, the M region consists of marine humic-like substances – encompassing a range of marine phytoplankton metabolites – and may be a possible photoproduct (Kieber et al., 2006a; Romera-Castillo et al., 2011; Chen et al., 2013). Given the observed increases in fluorescence in the M region upon photo-exposure and subsequent decrease in lability experiments, the M peak is a highly relevant fluorophore for investigation of photo-exposed estuarine sediments, as the turnover of compounds characterized by this peak may be rapid in estuaries experiencing disturbances.

The focus on lability in the current study, rather than bioavailability, is because abiotic factors may contribute to observed differences across treatments. While we were not able to attribute changes unequivocally to biological degradation, the greatest effects of lability were observed from the more bioavailable fluorophores (peaks M and T; (Cory and Kaplan, 2012; Chen et al., 2013)). Similar photo-bio-incubation studies tracking biological oxygen demand (BOD) of photo-exposed DOC exhibited biodegradation with four times less inoculum (Moran et al., 2000), supporting the suggestion that photo-labile DOC presented in this study is likely also bioavailable.

4.3. Environmental relevance of PR-DOM lability

The environmental significance of PR-DOM from resuspended sediments can be assessed by comparing labile PR-DOC in our experiments to ambient bioavailable DOC (BDOC) values in the CFRE. Assuming a DOC concentration in the CFRE of 200 μM C (Avery et al., 2003), a 9% bioavailability, and minimal biodegradation during estuarine transport (given short flushing times of 1–22 days) (Ensign et al., 2004), a parcel of water at the saltwater end-member under ambient conditions would contain 18 μM of BDOC.

Photo-induced changes in DOC concentration over the course of the lability incubations were normalized to the amount of TSS in the resuspension mixture using the equation below in order to determine the relative amount of labile DOC caused by photochemical release.

$$\text{Labile DOC } (\mu\text{molC g}^{-1}) = \frac{\Delta\text{DOC}(\mu\text{MC})}{\text{TSS}(\text{gL}^{-1})} \quad (1)$$

After 1 month, DOC decreased by an average of 7 μM more in light-exposed incubations, relative to unexposed incubations (Supplemental Table A). With an estimated TSS of 160 mg L^{-1}, there was an average labile DOC concentration of 44 μmol C g^{-1} of sediment added to the resuspension mixture in light-exposed flasks. While ambient TSS values in the CFRE are low (<50 mg L^{-1}), TSS concentrations during perturbations such as hurricanes or 1.5 year floods can reach 200–325 mg L^{-1} (Riggsbee et al., 2008; Chen et al., 2009). Assuming a moderate resuspension TSS amount of 100 mg L^{-1} the amount of labile PR-DOC after 6 h of irradiation would be 4.3 μM C. During higher energy resuspension events (TSS ~ 200 mg L^{-1}), labile PR-DOC is estimated to be much higher (8.6 μM C). Depending on the size and composition of suspended sediments, light attenuation coefficients can increase dramatically with TSS (doubling, for example, during Hurricane Fran in 1996) (Mallin et al., 2002) and may limit the extent of initial PR-DOC from sediments. However, photo-alteration is prevalent even in systems with high attenuation coefficients (Cory et al., 2015), and increased light penetration due to rapid large-particle settling can aid photo-exposure of fine sediments that may stay suspended for a week or more (Ralston and Geyer, 2017). Furthermore, increased surface area of fine sediments may increase their sensitivity to photorelease, depending on physicochemical conditions in the estuary (Mayer, 1994; Kieber et al., 2006b). Our estimates of labile PR-DOC are nearly half of the 18 μM of BDOC reported by Avery et al. (2003) and imply that in high energy resuspension events photochemical interactions with sediments may be a non-trivial contributor to labile DOC.

The relevance of labile PR-DOC can also be assessed on a basin-wide scale. Long Bay off the southeastern coast of North Carolina receives the majority of CFRE flow. The yearly amount of BDOC supplied by the CFRE to Long Bay is 7×10^9 g C yr^{-1} (Avery et al., 2003). Photochemical production of DOC from resuspended sediments rivals that of riverine discharge as a source of oceanic DOC, which is the largest surficial reservoir of organic carbon on Earth (Hedges, 1992; Kieber et al., 2006b). Under hurricane conditions the majority of Long Bay would be turbid and subject to increased sedimentary discharge from the CFRE. Applying the previous labile PR-DOC calculation to a high energy resuspension event (0.86 mmol C m^{-2} for 6 h of irradiation) for a TSS of 200 mg L^{-1} to the 10,000 km^2 area of Long Bay, results in photochemical production of 10×10^7 g C in one solar day. This would account for 1.5% of all BDOC provided by the CFRE to Long Bay reported for the entire year (Avery et al., 2003). Six days of resuspension and adequate sunlight would provide nearly 10% of all CFRE BDOC to the study site for the year. PR-DOC may therefore be a significant reservoir of labile material for bacteria and plankton in the CFRE, particularly during the summer months when tropical storms and hurricanes are common occurrences.

5. Conclusions

The irradiation of estuarine sediments released 22–44% more DOC than unirradiated controls. While some of the photo-released DOM was photohumified (higher molecular weight, higher aromaticity), N- and S-containing compounds were either photodegraded or biologically altered (lower molecular weight, lower aromaticity), allowing for enhanced photo-lability of PR-DOM, particularly for compounds fluorescing in the M region. In the CFRE, estimated labile PR-DOC from resuspension events (7–15 μM) is comparable to BDOC estimates (18 μM), demonstrating that PR-DOC during a resuspension event may be a substantial, previously unrecognized, source of labile DOC to bacteria and plankton in coastal environments.

Declaration of Competing Interest

The authors declare that they have no known competing financial interests or personal relationships that could have appeared to influence the work reported in this paper.

Acknowledgements

The authors would like to thank Yuri. E. Corilo for EnviroOrg™ development. We also gratefully acknowledge two anonymous reviewers whose comments and suggestions helped to improve this manuscript. Financial support of this project was provided by the National Science Foundation (NSF) Division of Chemical Oceanography (OCE-1154850), the NSF Division of Materials Research (DMR-11-57490), and the NSF Division of Chemistry (CHE-1039784).

Data availability

Datasets related to this article can be found on the data repository, Mendeley Data (https://doi.org/10.17632/g228pkdcym.1).

Appendix A. Supplementary material

Supplementary data to this article can be found online at https://doi.org/10.1016/j.orggeochem.2020.104164.

Associate Editor—**Sylvie Derenne**

References

Avery Jr., G.B., Willey, J., Kieber, R., Shank, G., Whitehead, R., 2003. Flux and bioavailability of Cape Fear River and rainwater dissolved organic carbon to Long Bay, southeastern United States. Global Biogeochemical Cycles - Global Biogeochem Cycle 17. https://doi.org/10.1029/2002GB001964.

Avery, G.B., Mickler, W., Probst, E., Mead, R.N., Skrabal, S.A., Kieber, R.J., David Felix, J., 2017. Photochemical release of sediment bound brevetoxin (PbTx-2) from resuspended sediments. Marine Chemistry 189, 25–31.

Azam, F., Fenchel, T., Field, J., Gray, J., Meyer-Reil, L., Thingstad, F., 1983. The Ecological Role of Water-Column Microbes in the Sea. Marine Ecology Progress Series 10, 257–263.

Biers, E.J., Zepp, R.G., Moran, M.A., 2007. The role of nitrogen in chromophoric and fluorescent dissolved organic matter formation. Marine Chemistry 103, 46–60.

Blakney, G.T., Hendrickson, C.L., Marshall, A.G., 2011. Predator data station: A fast data acquisition system for advanced FT-ICR MS experiments. International Journal of Mass Spectrometry, Special Issue. In Honor of Tino Gaumann 306, 246–252.

Blanton, J., Alexander, C., Alber, M., Kineke, G., 1999. The mobilization and deposition of mud deposits in a coastal plain estuary. Limnologica 29, 293–300.

Booth, J.G., Miller, R.L., McKee, B.A., Leathers, R.A., 2000. Wind-induced bottom sediment resuspension in a microtidal coastal environment. Continental Shelf Research 20, 785–806.

Boye, K., Noël, V., Tfaily, M.M., Bone, S.E., Williams, K.H., Bargar, J.R., Fendorf, S., 2017. Thermodynamically controlled preservation of organic carbon in floodplains. Nature Geoscience 10, 415–419.

Brogi, S.R., Ha, S.-Y., Kim, K., Derrien, M., Lee, Y.K., Hur, J., 2018. Optical and molecular characterization of dissolved organic matter (DOM) in the Arctic ice core and the underlying seawater (Cambridge Bay, Canada): Implication for increased autochthonous DOM during ice melting. Science of the Total Environment 627, 802–811.

Chen, H., Meng, W., Zheng, B., Wang, C., An, L., 2013. Optical signatures of dissolved organic matter in the watershed of a globally large river (Yangtze River, China). Limnologica 43, 482–491.

Chen, S., Huang, W., Wang, H., Li, D., 2009. Remote sensing assessment of sediment re-suspension during Hurricane Frances in Apalachicola Bay, USA. Remote Sensing of Environment 113, 2670–2681.

Cheng, Q., Zhuang, W.-E., Wang, H., Chen, W., Yang, L.-Y., 2019. [Spatial Distribution and Degradation of CDOM in the Minjiang River in Summer]. Huan Jing Ke Xue = Huanjing Kexue 40, 157–163.

Coble, P.G., 1996. Characterization of marine and terrestrial DOM in seawater using excitation-emission matrix spectroscopy. Marine Chemistry 51, 325–346.

Cory, R.M., Crump, B.C., Dobkowski, J.A., Kling, G.W., 2013. Surface exposure to sunlight stimulates CO2 release from permafrost soil carbon in the Arctic. Proceedings of the National Academy of Sciences 110, 3429–3434.

Cory, R.M., Harrold, K.H., Neilson, B.T., Kling, G.W., 2015. Controls on dissolved organic matter (DOM) degradation in a headwater stream: the influence of photochemical and hydrological conditions in determining light-limitation or substrate-limitation of photo-degradation. Biogeosciences 12, 6669–6685.

Cory, R.M., Kaplan, L.A., 2012. Biological lability of streamwater fluorescent dissolved organic matter. Limnology and Oceanography 57, 1347–1360.

Cory, R.M., Kling, G.W., 2018. Interactions between sunlight and microorganisms influence dissolved organic matter degradation along the aquatic continuum. Limnology and Oceanography Letters 3, 102–116.

Dittmar, T., Koch, B., Hertkorn, N., Kattner, G., 2008. A simple and efficient method for the solid-phase extraction of dissolved organic matter (SPE-DOM) from seawater. Limnology and Oceanography: Methods 6, 230–235.

Ensign, S.H., Halls, J.N., Mallin, M.A., 2004. Application of digital bathymetry data in an analysis of flushing times of two large estuaries. Computers & Geosciences 30, 501–511.

Findlay, S., Sinsabaugh, R.L., 2003. Aquatic Ecosystems: Interactivity of Dissolved Organic Matter. Academic Press.

Gonsior, M., Peake, B.M., Cooper, W.T., Podgorski, D., D'Andrilli, J., Cooper, W.J., 2009. Photochemically induced changes in dissolved organic matter identified by ultrahigh resolution Fourier transform ion cyclotron resonance mass spectrometry. Environmental Science & Technology 43, 698–703.

Hansell, D.A., Carlson, C.A., Repeta, D.J., Schlitzer, R., 2009. Dissolved organic matter in the ocean a controversy stimulates new insights. Oceanography 22, 202–211.

Hawkes, J.A., D'Andrilli, J., Agar, J.N., Barrow, M.P., Berg, S.M., Catalán, N., Chen, H., Chu, R.K., Cole, R.B., Dittmar, T., Gavard, R., Gleixner, G., Hatcher, P.G., He, C., Hess, N.J., Hutchins, R.H.S., Ijaz, A., Jones, H.E., Kew, W., Khaksari, M., Lozano, D. C.P., Lv, J., Mazzoleni, L., Noriega-Ortega, B.E., Osterholz, H., Radoman, N., Remucal, C.K., Schmitt, N.D., Schum, S., Shi, Q., Simon, C., Singer, G., Sleighter, R. L., Stubbins, A., Thomas, M.J., Tolic, N., Zhang, S., Zito, P., Podgorski, D.C., 2020. An international laboratory comparison of dissolved organic matter composition by high resolution mass spectrometry: Are we getting the same answer? Limnology and Oceanography: Methods. 18, 235–258. https://doi.org/10.1002/lom3.10364.

Hedges, J.I., 1992. Global biogeochemical cycles: progress and problems. Marine Chemistry 39, 67–93.

Helms, J.R., Glinski, D.A., Mead, R.N., Southwell, M.W., Avery, G.B., Kieber, R.J., Skrabal, S.A., 2014. Photochemical dissolution of organic matter from resuspended sediments: Impact of source and diagenetic state on photorelease. Organic Geochemistry 73, 83–89.

Helms, J.R., Stubbins, A., Ritchie, J.D., Minor, E.C., Kieber, D.J., Mopper, K., 2008. Absorption spectral slopes and slope ratios as indicators of molecular weight, source, and photobleaching of chromophoric dissolved organic matter. Limnology and Oceanography 53, 955–969.

Herlemann, D.P.R., Manecki, M., Meeske, C., Pollehne, F., Labrenz, M., Schulz-Bull, D., Dittmar, T., Jürgens, K., 2014. Uncoupling of bacterial and terrigenous dissolved organic matter dynamics in decomposition experiments. PLoS ONE 9, e93945.

Hernes, P.J., Bergamaschi, B.A., Eckard, R.S., Spencer, R.G.M., 2009. Fluorescence-based proxies for lignin in freshwater dissolved organic matter. Journal of Geophysical Research: Biogeosciences 114. https://doi.org/10.1029/2009JG000938.

Hertkorn, N., Harir, M., Cawley, K.M., Schmitt-Kopplin, P., Jaffé, R., 2016. Molecular characterization of dissolved organic matter from subtropical wetlands: a comparative study through the analysis of optical properties, NMR and FTICR/MS. Biogeosciences 13, 2257–2277.

Hill, P.S., Milligan, T.G., Geyer, W.R., 2000. Controls on effective settling velocity of suspended sediment in the Eel River flood plume. Continental Shelf Research, Oceanic Flood Sedimentation 20, 2095–2111.

Huguet, A., Vacher, L., Relexans, S., Saubusse, S., Froidefond, J.M., Parlanti, E., 2009. Properties of fluorescent dissolved organic matter in the Gironde Estuary. Organic Geochemistry 40, 706–719.

Hunt, A.P., Parry, J.D., Hamilton-Taylor, J., 2000. Further evidence of elemental composition as an indicator of the bioavailability of humic substances to bacteria. Limnology and Oceanography 45, 237–241.

Jackson, M.L., 1973. Soil Chemical Analysis - Advanced Course. .

Judd, K.E., Crump, B.C., Kling, G.W., 200. Bacterial responses in activity and community composition to photo-oxidation of dissolved organic matter from soil and surface waters. Aquatic Sciences 69, 96–107.

Kaiser, N.K., Quinn, J.P., Blakney, G.T., Hendrickson, C.L., Marshall, A.G., 2011. A Novel 9.4 Tesla FTICR mass spectrometer with improved sensitivity, mass resolution, and mass range. Journal of The American Society for Mass Spectrometry 22, 1343–1351.

Kellerman, A.M., Dittmar, T., Kothawala, D.N., Tranvik, L.J., 2014. Chemodiversity of dissolved organic matter in lakes driven by climate and hydrology. Nature Communications 5, 3804.

Kieber, R.J., Hartrey, L.M., Felix, D., Corzine, C., Avery, G.B., Mead, R.N., Skrabal, S.A., 2017. Photorelease of microcystin-LR from resuspended sediments. Harmful Algae 63, 1–6.

Kieber, R.J., Hydro, L.H., Seaton, P.J., 1997. Photooxidation of triglycerides and fatty acids in seawater: Implication toward the formation of marine humic substances. Limnology and Oceanography 42, 1454–1462.

Kieber, R.J., Whitehead, R.F., Reid, S.N., Willey, J.D., Seaton, P.J., 2006a. Chromophoric Dissolved Organic Matter (CDOM) In Rainwater, Southeastern North Carolina, USA. Journal of Atmospheric Chemistry 54, 21–41.

Kieber, R.J., Whitehead, R.F., Skrabal, S.A., 2006b. Photochemical production of dissolved organic carbon from resuspended sediments. Limnology and Oceanography 51, 2187–2195.

Kim, S., Kaplan, L.A., Hatcher, P.G., 2006. Biodegradable dissolved organic matter in a temperate and a tropical stream determined from ultra-high resolution mass spectrometry. Limnology and Oceanography 51, 1054–1063.

Koch, B.P., Dittmar, T., 2006. From mass to structure: an aromaticity index for high-resolution mass data of natural organic matter. Rapid Communications in Mass Spectrometry 20, 926–932.

Kowalczuk, P., Cooper, W.J., Whitehead, R.F., Durako, M.J., Sheldon, W., 2003. Characterization of CDOM in an organic-rich river and surrounding coastal ocean in the South Atlantic Bight. Aquatic Sciences 65, 384–401.

Lønborg, C., Nieto-Cid, M., Hernando-Morales, V., Hernández-Ruiz, M., Teira, E., Álvarez-Salgado, X.A., 2016. Photochemical alteration of dissolved organic matter and the subsequent effects on bacterial carbon cycling and diversity. FEMS Microbiology Ecology 92. https://doi.org/10.1093/femsec/fiw048.

Mallin, M.A., McIver, M.R., Merritt, J., F., 2015. Environmental Assessment of the Lower Cape Fear River System, 2015 (No. 16– 02). University of North Carolina, Wilmington, Center for Marine Sciences.

Mallin, M.A., Posey, M.H., McIver, M.R., Parsons, D.C., Ensign, S.H., Alphin, T.D., 2002. Impacts and Recovery from Multiple Hurricanes in a Piedmont-Coastal Plain River SystemHuman development of floodplains greatly compounds the impacts of hurricanes on water quality and aquatic life. BioScience 52, 999–1010.

Mayer, L., Thornton, K., Schick, L., 2011. Bioavailability of organic matter photodissolved from coastal sediments. Aquatic Microbial Ecology 64, 275–284.

Mayer, L.M., 1994. Surface area control of organic carbon accumulation in continental shelf sediments. Geochimica et Cosmochimica Acta 58, 1271–1284.
Mayer, L.M., Schick, L.L., Skorko, K., Boss, E., 2006. Photodissolution of particulate organic matter from sediments. Limnology and Oceanography 51, 1064–1071.
McKnight, D.M., Boyer, E.W., Westerhoff, P.K., Doran, P.T., Kulbe, T., Andersen, D.T., 2001. Spectrofluorometric characterization of dissolved organic matter for indication of precursor organic material and aromaticity. Limnology and Oceanography 46, 38–48.
Mopper, K., Kieber, D., 2002. Photochemistry and the cycling of carbon, sulfur, nitrogen and phosphorus. Biogeochemistry of Marine Dissolved Organic Matter., 455–507
Mopper, K., Kieber, D.J., Stubbins, A., 2015. Chapter 8 - Marine Photochemistry of Organic Matter: Processes and Impacts. In: Hansell, D.A., Carlson, C.A. (Eds.), Biogeochemistry of Marine Dissolved Organic Matter. second ed. Academic Press, Boston, pp. 389–450.
Moran, M.A., Sheldon, W.M., Zepp, R.G., 2000. Carbon loss and optical property changes during long-term photochemical and biological degradation of estuarine dissolved organic matter. Limnology and Oceanography 45, 1254–1264.
Ohno, T., 2002. Fluorescence inner-filtering correction for determining the humification index of dissolved organic matter. Environmental Science & Technology 36, 742–746.
Osburn, C.L., Wigdahl, C.R., Fritz, S.C., Saros, J.E., 2011. Dissolved organic matter composition and photoreactivity in prairie lakes of the U.S. Great Plains. Limnology and Oceanography 56, 2371–2390.
Perez, B.C., Day, J.W., Rouse, L.J., Shaw, R.F., Wang, M., 2000. Influence of Atchafalaya River Discharge and Winter Frontal Passage on Suspended Sediment Concentration and Flux in Fourleague Bay, Louisiana. Estuarine, Coastal and Shelf Science 50, 271–290.
Ralston, D.K., Geyer, W.R., 2017. Sediment transport time scales and trapping efficiency in a Tidal River. Journal of Geophysical Research: Earth Surface 122, 2042–2063.
Reche, I., Pulido-Villena, E., Conde-Porcuna, J.M., Carrillo, P., 2001. Photoreactivity of dissolved organic matter from high-mountain lakes of Sierra Nevada, Spain. Arctic Antarctic and Alpine Research 33, 426–434.
Reitner, B., Herzig, A., Herndl, G., 2002. Photoreactivity and bacterioplankton availability of aliphatic versus aromatic amino acids and a protein. Aquatic Microbial Ecology 26, 305–311.
Riedel, T., Biester, H., Dittmar, T., 2012. Molecular fractionation of dissolved organic matter with metal salts. Environmental Science & Technology 46, 4419–4426.
Riggsbee, J.A., Orr, C.H., Leech, D.M., Doyle, M.W., Wetzel, R.G., 2008. Suspended sediments in river ecosystems: Photochemical sources of dissolved organic carbon, dissolved organic nitrogen, and adsorptive removal of dissolved iron. Journal of Geophysical Research: Biogeosciences 113. https://doi.org/10.1029/2007JG000654.
Romera-Castillo, C., Sarmento, H., Álvarez-Salgado, X.A., Gasol, J.M., Marrasé, C., 2011. Net production and consumption of fluorescent colored dissolved organic matter by natural bacterial assemblages growing on marine phytoplankton exudates▽. Applied and Environmental Microbiology 77, 7490–7498.
Savory, J.J., Kaiser, N.K., McKenna, A.M., Xian, F., Blakney, G.T., Rodgers, R.P., Hendrickson, C.L., Marshall, A.G., 2011. Parts-per-billion Fourier transform ion cyclotron resonance mass measurement accuracy with a "walking" calibration equation. Analytical Chemistry 83, 1732–1736.
Schiebel, H.N., Wang, X., Chen, R.F., Peri, F., 2015. Photochemical release of dissolved organic matter from resuspended salt marsh sediments. Estuaries and Coasts 38, 1692–1705.
Seidel, M., Yager, P.L., Ward, N.D., Carpenter, E.J., Gomes, H.R., Krusche, A.V., Richey, J.E., Dittmar, T., Medeiros, P.M., 2015. Molecular-level changes of dissolved organic matter along the Amazon River-to-ocean continuum. Marine Chemistry, Biogeochemistry of Dissolved Organic Matter 177, 218–231.
Shank, G.C., Evans, A., Yamashita, Y., Jaffé, R., 2011. Solar radiation–enhanced dissolution of particulate organic matter from coastal marine sediments. Limnology and Oceanography 56, 577–588.
Skrabal, S.A., McBurney, A.M., Webb, L.A., Brooks Avery Jr., G., Kieber, R.J., Mead, R. N., 2018. Photodissolution of copper from resuspended coastal marine sediments. Limnology and Oceanography 63, 773–785.
Southwell, M.W., Mead, R.N., Luquire, C.M., Barbera, A., Avery, G.B., Kieber, R.J., Skrabal, S.A., 2011. Influence of organic matter source and diagenetic state on photochemical release of dissolved organic matter and nutrients from resuspendable estuarine sediments. Marine Chemistry 126, 114–119.
Spencer, R.G.M., Guo, W., Raymond, P.A., Dittmar, T., Hood, E., Fellman, J., Stubbins, A., 2014. Source and biolability of ancient dissolved organic matter in glacier and lake ecosystems on the Tibetan Plateau. Geochimica et Cosmochimica Acta 142, 64–74.
Stedmon, C.A., Nelson, N.B., 2015. Chapter 10 - The Optical Properties of DOM in the Ocean. In: Hansell, D.A., Carlson, C.A. (Eds.), Biogeochemistry of Marine Dissolved Organic Matter. second ed. Academic Press, Boston, pp. 481–508.
Stubbins, A., Spencer, R.G.M., Chen, H., Hatcher, P.G., Mopper, K., Hernes, P.J., Mwamba, V.L., Mangangu, A.M., Wabakanghanzi, J.N., Six, J., 2010. Illuminated darkness: Molecular signatures of Congo River dissolved organic matter and its photochemical alteration as revealed by ultrahigh precision mass spectrometry. Limnology and Oceanography 55, 1467–1477.
Sun, L., Perdue, E.M., Meyer, J.L., Weis, J., 1997. Use of elemental composition to predict bioavailability of dissolved organic matter in a Georgia river. Limnology and Oceanography 42, 714–721.
Tranvik, L.J., Bertilsson, S., 2001. Contrasting effects of solar UV radiation on dissolved organic sources for bacterial growth. Ecology Letters 4, 458–463.
Wasmund, K., Mußmann, M., Loy, A., 2017. The life sulfuric: microbial ecology of sulfur cycling in marine sediments. Environmental Microbiology Reports 9, 323–344.
Weishaar, J.L., Aiken, G.R., Bergamaschi, B.A., Fram, M.S., Fujii, R., Mopper, K., 2003. Evaluation of specific ultraviolet absorbance as an indicator of the chemical composition and reactivity of dissolved organic carbon. Environmental Science & Technology 37, 4702–4708.
Yang, H., Li, B., Zhang, C., Qiao, H., Liu, Y., Bi, J., Zhang, Z., Zhou, F., 2020. Recent spatio-temporal variations of suspended sediment concentrations in the Yangtze Estuary. Water 12, 818.
Zhang, J., 1999. Heavy metal compositions of suspended sediments in the Changjiang (Yangtze River) estuary: significance of riverine transport to the ocean. Continental Shelf Research 19, 1521–1543.